RSC Advances

ROYAL SOCIETY OF CHEMISTRY

www.rsc.org/advances

Combined DFT and experimental study of the dispersion and interaction of copper species in Ni-CeO_2 nanosized solid solutions

*Eugenio F. de Souza[1], Carlos Alberto Chagas[1], Robinson L. Manfro[3], Mariana M.V.M. Souza[3], Ricardo Bicca de Alencastro[2], Martin Schmal[1]**

[1] Universidade Federal do Rio de Janeiro, Núcleo de Catálise, Programa de Engenharia Química, COPPE.
Av. Horácio Macedo, 2030 - Centro de Tecnologia - Bloco G - Ilha do Fundão
21941-914 - Rio de Janeiro, RJ - Brasil - Caixa-postal: 68502
Tel: (21) 3938-8137

[2] Universidade Federal do Rio de Janeiro. Rio de Janeiro, Instituto de Química. Programa de PG em Química. Laboratorio de Modelagem Molecular-LABMMOL Av. Athos da Silveira Ramos No 149, CT, Bloco A, sala 609. tel: (21) 2562-7132 - fax: (21) 2562-7132

[3] Escola de Química, Universidade Federal do Rio de Janeiro, Centro de Tecnologia, Bloco E, sala 206, CEP 21941-909, Rio de Janeiro/RJ, Brasil

*corresponding author: **schmal@peq.coppe.ufrj.br**

ABSTRACT: Nanosized nickel (Ni) and copper (Cu) doped ceria (CeO_2) have attracted attention as solid solutions for energy- and environment-related applications. Furthermore they present an interesting combination of thermal and chemical stability and catalytic activity in technologically important reactions like water gas shift, ethanol reforming, hydrogenation, among others. In contrast, not much is known about the key-factors that govern the formation and the nature of the atomic structure of these materials. This study investigated with the help of the density functional theory (DFT) and experimental methodologies the formation of ceria-based solid solutions in the presence of Ni and Cu species. The materials were prepared by the incipient wetness impregnation and subsequently characterized by various experimental techniques (XPS, Raman, XRD, XRF, HR-TEM), while the electronic structures have been investigated by using DFT calculations with Hubbard corrections (DFT+U method). Theoretical calculations and experimental studies suggest that Ni species are able to form a solid solution by isomorphic substitution of bulk Ce atoms, however it was found a limit after which saturation is reached and therefore the addition of extra Ni atoms do not affect the crystal structure of the solid solution. Consequently, the formation of surface domains of nickel oxide (NiO) phases is expected. According to our findings the addition of small amounts of Cu can neither disturb the bulk structure nor force the incorporation of Cu atoms and therefore Cu species are also expected to segregated oxide (CuO). Our theoretical approach is consistent with the experimental data and we could identify an idealized solid solution structure that presents a close similarity with the experimental findings. From this theoretical structure, an interaction of the type Ni-Ni pair was identified. Our theoretical studies have predicted lattice contraction as a function of the Ni loading. From an energetic point of view we show that small amounts of Ni are easily incorporated whereas by raising Ni concentration and by adding Cu a sharp increase of the formation energy is observed. High formation energies along with strong lattice contractions was associated as plausible causes for the segregation of both Ni and Cu oxides and have been suggested as simple indicators of key factors for tailoring doped oxides containing controlled dopant concentrations.

KEYWORDS: Ceria, solid solutions, Cu, Ni, nanomaterials, DFT+U

1. INTRODUCTION

The development of nanostructured materials for applications in heterogeneous catalysis has been the target of great interest in recent years. In particular, nanosized cerium oxide or ceria (CeO_2) represent an important class of rare metal oxides attracting great attention due to its unique physical and chemical properties, serving as a low-cost alternative to numerous applications in nanocatalysis.[1–3] Because of its high thermal and mechanical stability, excellent redox properties and exceptional oxygen storage capacity, ceria has been widely used as support for various noble and "non-noble" catalysts,[4–9] whereas ceria itself is also utilized as an excellent catalyst for a number of important reactions.[10–13] Besides versatile one of its most interesting characteristics rely on the capacity of forming solid solutions of the type $Ce_{1-x}E_xO_2$ *via* substitutional doping (or isomorphic substitution of Ce by "E"), in which "E" might be various elements, generally transition metals (TM) such as Cu, Ni, La, Gd, Eu, Pt, Au, Ru, *etc*.[14–18] Importantly, these solid solutions are capable of maintaining ceria fluorite-like structure even under high concentrations of dopants, where "x" usually ranges from 0.01 to 0.5.

Especially in the field of heterogeneous catalysis a number of preparation methods have been studied since secondary and ternary (two metals plus Ce) solid solutions were found to substantially enhance the performance of ceria-based catalysts. Among the most studied, nickel (Ni) doped ceria (Ni-CeO_2) is known for its outstanding catalytic properties as well as for its thermal and chemical stability, being used in important reactions such as water gas shift (WGS),[19] CH_4 and CO oxidation,[20] ethanol reforming and hydrogenation processes, *etc.*[21,22] Moreover, the Ni-CeO_2 catalytic activity can be further improved through the incorporation of a second TM, which promotes modifications at electronic and structural levels. In special the addition of Cu has shown very interesting catalytic properties, being demonstrated for example that Cu-modified Ni-CeO_2 catalysts are able to suppress methane formation in WGS reactions, presenting high resistance to carbon deposition.[9,23,24] The substantial increase in the activity and structural stability of Ni-CeO_2

and Cu-modified Ni-CeO_2 catalysts are credited to a combined effect between host and dopants, which in turn is inherently governed by atomic-level mechanisms. However, the formation and the nature of the atomic structure of these materials have not been deeply investigated and for that reason a joint study based on experimental techniques and Density Functional Theory (DFT) might be of enormous utility. Although less extensive than the vast experimental literature on TM-doped ceria, in recent years DFT investigations have given valuable contributions on qualitative and even quantitative terms. Together with modern experimental methods, DFT calculations are now able to guide researchers in their quest for improved (non-empirical) ceria-based materials, providing a detailed atomistic knowledge regarding composition and morphology.[25] For example, a particularly difficult challenge, independently of the preparation method, is to understand how solid solutions are formed and why different phases segregate (after reaching a solubility "limit").[26] In particular, considering the interaction of Ni and Cu with ceria a few questions arise: (i) in which extension the ceria lattice is disturbed? (ii) How (bulk) chemical interactions take place? (iii) How the concomitant presence of two metals affects the system as a whole?

As the intrinsic complexity of the atomic structure makes the answers difficult to find by only using experimental methodologies, in this paper we employ a combined experimental and DFT approach in order to gain fundamental understanding on the ceria-based compounds through the investigation of the formation of Ni-CeO_2 and Cu-modified Ni-CeO_2. Accordingly, our focus is concentrated on the components (mainly structural and energetic factors) that control the formation of solid solutions, concerning several interesting experimental and theoretical aspects. In fact, more knowledge and information at the atomic level is essential and fundamental in tuning the desired catalytic (or other) properties of advanced ceria-based materials. In the present study, our experimental and theoretical results revealed that the Ce/Ni exchange forming a solid solution is limited and modulated by energetic (increasing formations energies) and structural (lattice shrinking) factors. Furthermore, despite a second metal (Cu) possesses no influence in the solid

solution (it was segregated due to the high energetic costs involved in the incorporation of Cu into the lattice), it was hypothesized that the presence of Cu species on the surface of the grains would be one of the reasons for the improved activity of the ceria-based catalysts, due to the formation of Ni-Cu alloys.[19]

We firmly believe that the results presented here may be useful and principally they might be extensible to other oxide-based systems, providing a fertile ground where strategies to the synthesis and tailoring of better catalytic doped-materials with well controlled dopant concentrations might be devised *via* theoretical calculations. The paper will be organized as follows: the experimental methodology and the characterization techniques are presented in Subsections 2.1 and 2.2, respectively. The computational setup and the theoretical models are presented in Subsections 3.1 and 3.2. In turn, our results are split into two main parts: experimental (Subsection 4.1) and theoretical (Subsection 4.2). Lastly, in Sections 5 and 6 we provide our concluding remarks and references used along the paper, respectively.

2. EXPERIMENTAL SECTION

2.1 – Preparation of the Nanomaterials

Nanosized Ni-CeO_2 and Cu-modified Ni-CeO_2 were synthesized *via* incipient wetness impregnation.[27] Firstly, CeO_2 was obtained by calcining $Ce(NO_3)_3.6H_2O$ in air at 500 °C during 3h. Ni was further incorporated through an aqueous solution of the precursor salt, $Ni(NO_3)_2$. Then, the sample was dried at 110 °C overnight followed by calcination at 500 °C in air for 3h in order to form the Ni-CeO_2 system. The addition of Cu to Ni-CeO_2 was conducted *via* sequential impregnation with aqueous solution of $Cu(NO_3)_3$. Subsequently, the sample was dried and calcined similarly. The nominal loading of Ni is 20 wt.% while the amount of Cu is 6 wt. %. In this paper we opted to evaluate only the presence of small amounts of Cu based on the fact that diffraction peaks relative to CuO were not identified in a study involving Cu-modified ceria of similar composition (3-5% of Cu), which in turn suggested the formation of a solid solution.[47] However, we will show

that it is not necessarily true considering the concomitant presence of nickel. The synthesized Ni-CeO_2 and Cu-modified Ni-CeO_2 materials from now on will be referred as $NiCeO_\delta$ and Cu-$NiCeO_\delta$, respectively, in which δ aim at the possible presence of O defects as observed in experimentally synthesized oxides and doped oxides.[26]

2.2 – Characterization

Powder X-ray diffraction (XRD) measurements were performed using a Rigaku Miniflex diffractometer equipped with a graphite monochromator operated at 30 kV and 15 mA, using CuKα radiation (λ =1.5406 Å). The measurements were carried out with a step size of 0.05° and counting time of 1s per step, reproduced here without any background or smoothing treatment. The structures were subsequently refined by the Rietveld technique.[28] Analyses of the chemical composition were performed by X-ray fluorescence (XRF) using a Rigaku RIX 3100 spectrometer. Raman spectra were collected at room temperature using a LabRam HR-UV800/Jobin-Yvon spectrometer equipped with a He–Ne laser (λ = 632 nm), thermal conductivity detector (T = -70 °C) and an Olympus BX41 microscope (where 3-5 regions were analyzed). The surface chemical state of the atoms and their relative abundance were evaluated by X-ray photoelectron spectroscopy (XPS) using a ESCALAB 250 spectrometer (Thermo Scientific), employing monochromatic AlKα (1486.6 eV) as the X-ray source. The XPS data was collected at pressures normally on the order of 10^{-8} Torr and ambient temperature. The binding energies were calibrated internally by carbon deposit with C 1s at 284.6 eV. Spectra were analyzed using a Gaussian-Lorenzian peak shape obtained from CasaXPS software. Atomic ratios were quantitatively analyzed by determining the areas of the elemental peaks through the Shirley background subtraction as usually documented in the literature. Scanning transmission electron microscopy (STEM) images were obtained on a FEI Titan 80-300 microscope operated at 300 kV. The samples were prepared by dispersion in water and spread onto a carbon-coated Cu grid.

3. COMPUTATIONAL METHODOLOGY

3.1 – Computational Setup

Our theoretical calculations were performed within the framework of the DFT using the plane-wave total-energy method. The PWSCF computational code was employed as implemented in the Quantum-ESPRESSO (QE) suite of programs.[29] The Perdew-Burke-Ernzerhof (PBE) form of the generalized gradient approximation[30] was used to calculate the exchange and correlation contributions while core-valence electron interactions were described by ultrasoft pseudopotentials.[31] The Kohn-Sham electronic states were expanded in plane-waves up to a kinetic energy cutoff of 40 Ry (1 Ry ~ 13.6 eV) and 400 Ry for the charge density cutoff. Self-consistency was achieved when the force applied on each atom according to the Hellmann-Feynman approximation was less than 1 x 10^{-3} Ry/Bohr and the variation of the total energy between two consecutive iterations was on the order of 1 x 10^{-4} Ry. Integrals over the Brillouin-zone were performed only at the Γ-point using a Gaussian smearing of 0.01 Ry, in a good compromise between computational cost and accuracy. During structural optimization the BFGS algorithm[32] was applied and both atomic positions and lattice vectors were allowed to simultaneously relax. All calculations were performed considering spin-polarization effects.

It is known that standard DFT functionals like PBE often fail in the accurate description of atoms with strongly correlated electrons.[33] This is generally associated to an incomplete treatment of correlation effects and self-interaction errors. Therefore, in this paper we have chosen to use the DFT plus U (DFT+U) method aiming at a more accurate description of the electronic properties of the ceria-based materials.[34] In this method a Hubbard-like term (+U) is introduced in order to correctly describe the on-site Coulomb repulsion, leading to a more realistic localization of *f*-electrons on Ce atoms. Despite widely used, a number of studies have shown that the +U parameter is not unambiguously specified for cerium oxides and an appropriate value is not unique.[25] Nevertheless, the literature shows that a +U value of 4.6 eV for Ce represent an excellent

approximation for doped oxides and satisfactorily suits our current problem.[34–36] Accordingly, a value of +U = 4.6 eV was used herein. Nevertheless, the evaluation of the formation energies as a function of the +U parameter value, besides a detailed analysis of the electronic structure of the solid solutions, are important for a deeper understanding of the properties of doped ceria and are presented in the Supporting Information as a separated section.

3.2 – Structure Models

Based on the optimized lattice parameter of the conventional cell, cubic (2x2x2) supercells comprising 32 units of CeO_2 (96 atoms each) were generated in order to represent realistic systems. Regarding the doping process, it is obvious that dopants can either substitute Ce sites or occupy interstitial sites. However, the literature shows that interstitial positions are highly unlikely to be occupied in ceria-based materials because of the high energy necessary to place dopants in that positions.[35,39] For that reason, in the present study we have accounted only for substitutional dopants. From this point, various solid solutions could be exploited: considering Ni and Cu-doped cerias, namely $Ce_{1-x-y}Ni_xCu_yO_2$, "x" and "y" correspond to 0.0, 3.12, 6.25, 9.37, 12.5, 15.6 and 18.75% of isomorphic substitution, respectively. Then, the formation energy was calculated following:

$$\Delta E_f = [E(Ce_{1-x-y}Ni_xCu_yO_2) + mE(Ce)] - [E(CeO_2) + nE(Ni) + oE(Cu)]$$

The integers "m", "n" and "o" indicate the number of dopant according to the percentage of substitution. ΔE_f denotes the calculated formation energy, $E(Ce_{1-x-y}Ni_xCu_yO_2)$ represent the DFT+U total energy of the doped ceria, $E(CeO_2)$ is the total energy of the pure ceria supercell, whereas E(Ce), E(Ni) and E(Cu) represent the energies relative to the Ce, Ni and Cu atoms, respectively. It is important to notice that when Cu is not present (see 4.2.1) both "y" index and "o" integer have to be zero. The energies of the constituent metals are referred to their oxides and calculated according to the following equations: 1) E(Ce)=[E(CeO_2)-2E(O)]; 2) E(Ni)=[E(NiO)-(O)]; 3) E(Cu)=[E(CuO)-E(O)]. In order to compensate the well-known over binding of the O_2 molecule by using a standard

(PBE) functional, the energy of an oxygen atom [E(O)] can be defined through the equation $E(O)=E(H_2O)-E(H_2)$.[40]

It is important to emphasize that we are quite aware of the presence of intrinsic oxygen vacancies as a consequence of the formation of solid solutions.[25,41,42] The existence of O-vacant sites introduces an extra challenge to the simulations due to the broad number of possible configurations. However, it is known that formation energies are not significantly altered by the presence of oxygen vacancies in doped ceria.[35,41] Since we are interested in tendencies regarding formation energies, in our modeling we did not consider the existence of vacancies. In fact, such an approximation is more interesting for us because it evaluates only the effects caused by the presence of dopants, representing a first indicative of thermodynamic stability under oxidizing/reducing atmospheres. Because attention in that line are indeed important further theoretical calculations including O vacancies are now in progress in our laboratory, being the target of a future work. Our preliminary results indicate an O-vacancy formation energy of 2.43 eV, whereas the difference in the formation energies between doped ceria with and without O vacancy was found to be usually lesser than 0.1 eV. These results are in good agreement with the literature.[35,41,43]

4. RESULTS AND DISCUSSION

4.1 – Experimental

In Fig. 1 the well-resolved diffraction lines confirm the crystalline nature of the as-prepared materials. For pure CeO_2 the typical XRD peaks present an excellent correspondence with the standard fluorite-type crystal structure of ceria (JCPDS-340394), while impurities or precursor residues could not be detected. On the other hand, besides all peaks relative to CeO_2 the $NiCeO_\delta$ diffractogram includes others corresponding to the NiO phase (JCPDS-441159). Moreover, regarding Cu-$NiCeO_\delta$ two small peaks relative to CuO (JCPDS-481548) were also detected at 2θ around 35-40° as evidenced by a magnification of this region (see the inset graph in Fig. 1). Despite

the intrinsic presence of these oxides, the formation of solid solutions through the incorporation of Ni and Cu species into the CeO_2 lattice is feasible and has to be further investigated.

Figure 1

Table 1

In principle, the formation of solid solutions might be evaluated by observing variations of the lattice parameters and diffraction lines.[2] Thus, all XRD patterns were refined by means of the Rietveld method and the results are summarized in Table 1. Regarding pure and Ni-doped ceria, a slight decrease in the experimental lattice parameter (a_{EXP}), from 5.413 Å to 5.407 Å, was observed. Furthermore, exactly the same variation (Δa_{EXP} = -0.006 Å) was determined with respect to the Cu-modified $NiCeO_\delta$ system. This modest lattice contraction might be ascribed to the incorporation of a portion of the Ni atoms into the ceria crystal structure. Ideally, this is consistent with the substitution of Ce^{4+} (0.97 Å) by smaller ionic radius Ni^{2+} ions (0.72 Å). On the other hand, the lack of variation in the refined parameter indicates that the Cu atoms (added subsequently to $NiCeO_\delta$) were not incorporated into the lattice. Accordingly, our data indicate that Cu and the remaining Ni amount (not incorporated) form segregated CuO and NiO phases, respectively. In addition, no significant changes in the crystallite size were observed (see Table 1), suggesting that the incorporation of Ni would have a tendency to avoid the growth of ceria crystals.

Figure 2

Our previous assumptions were further supported by Raman experiments. As seen in Fig. 2, the main band around 462 cm^{-1} correspond to the triply degenerate F_{2g} symmetrical stretching mode of the Ce-O unit.[44,45] Nonetheless, this vibrational mode was slightly displaced towards lower relative wave numbers for both $NiCeO_\delta$ and Cu-modified $NiCeO_\delta$, suggesting that a solid solution was formed.[46] It is interesting to note that a shoulder around 500 cm^{-1} observed after the

incorporation of Ni and Cu might be ascribed to the presence of O defects, a well-known effect fostered by the doping process in oxides.[26] So far our results suggest that a portion of the Ni atoms were incorporated into the ceria lattice while the same would not be true for Cu, considering that a slight wave number displacement would be expected.[47] In this case, STEM images can be helpful to further understand the crystalline properties of these materials.

Fig. 3 depicted the TEM images relative to Cu-$NiCeO_{\delta}$ in which the interlayer distances obtained by Fast Fourier Transformation (FFT) shows fringes separated by ~2.7 Å (0.27 nm) and ~3.17 Å (0.317 nm) corresponding to the CeO_2(200) and CeO_2(111) planes of the fluorite-like structure, respectively;[46,48] similar conclusions can be drawn for $NiCeO_{\delta}$. However, although identified by XRD (Fig. 1) CuO could not be determined by STEM, suggesting a well-dispersed phase. The larger inset graph in Fig. 3 illustrates our theoretical model regarding the CeO_2 bulk (see Subsection 4.2 for further details), which presents an excellent agreement with experimental interlayer distances and confirms that the lattice structure was only slightly perturbed by the presence of Cu and Ni-related phases. It has been reported that crystalline phases like aggregated/dispersed NiO as well as Ni atoms incorporated by the CeO_2 lattice forming $Ce_{1-x}Ni_xO_2$ solid solutions may co-exist with ceria composite.[49] Accordingly, fringes separated by ~2.4 Å (0.24 nm) shown in Fig. 3 (smaller inset) and related to NiO [(111) plane] could be observed in combination with CeO_2 corroborating the presence of the two distinguished phases.

Figure 3

Since Fig. 3 shows no evidences for Cu-related phases, a complementary XPS analysis was used to probe the chemical environment of surface Ni and Cu atoms over $NiCeO_{\delta}$ and Cu-$NiCeO_{\delta}$. A typical survey-scan of Cu-$NiCeO_{\delta}$ presented in Fig. 4 (A), along with a magnification (inset graphs) of the XPS spectra relative to the Cu $2p_{3/2}$ (I) and Ni $2p_{3/2}$ (II) core regions, reveals the presence of both Ni and Cu species with corresponding surface compositions of 11.4% and 5.5%, respectively. These values are smaller when compared with the composition obtained by XRF (22

Ni% and 6 Cu%). This result suggests that ~10.6%, which is the difference between obtained by XRF and detected by XPS, of the Ni atoms were incorporated by the ceria lattice. The surface composition of Cu was found to be 5.5%, which is only slightly smaller than the nominal composition (6%). Accordingly, the XPS peaks located at 934.0 eV and 942.8 eV [the inset graph 'I' in Fig. 4 (A)] are related to the Cu 2p core level region being mostly attributable to the Cu^{2+} state of the corresponding oxide (CuO).[47,50] Interestingly, a survey-scan of the chemical composition of Cu-$NiCeO_{\delta}$ and $NiCeO_{\delta}$ (before the addition of Cu) shown in Fig. 4 [(A) and (B)] indicate that the amount of Ni is ~11.4% and ~17%, respectively; the difference between them (5.6%) is almost the same as the amount of Cu detected by XPS (5.5%). Such an analysis strongly suggests that practically all of Cu present would be covering Ni, both in the form of oxide. As also seen in Table 1 the crystallite size of CuO (293 Å) is larger than NiO (285 Å), which might help to explain the partial covering of NiO by CuO. Correspondingly, the peaks located in BE of 855.9 eV and 862.2 eV [the inset graph 'II' in Fig. 4 (A)] can be ascribed to electronic states of the Ni 2p core level regions being unambiguously ascribed to Ni in the 2+ oxidation state. So the small variation on the amount of Cu (~0.5%) detected by XPS compared to the nominal composition would be within the error bar of our analysis and possibly all of Cu present forms uniformly dispersed surface oxide instead of being incorporated into the lattice. On the other hand, metallic phases (Ni^0 and Cu^0) were not identified.

Figure 4

As seen, our previous analyses provided important information regarding the co-existence of a solid solution (Ce-Ni-O) as well as segregated nickel and copper oxide phases, however not much could be inferred about the local (atomic-level) structure of the systems under study. Besides, the literature available for similar systems mainly focuses on macroscopic properties and therefore limited information about the complex local atomic structure is given. Accordingly, Sham *et.al.*[49]

suggested that small sized or highly dispersed NiO phases are present in elevated Ni concentrations (>30%), co-existing with CeO_2 and $Ce_{1-x}Ni_xO_2$ solid solutions, in good agreement with our data. Fang *et.al.*[51] also observed diffraction peaks related to the presence of NiO nanoparticles on ceria with Ni content higher than ~13 wt%, whereas Pino and co-workers[52] confirm the existence of well-crystallized NiO on $Ce_{1-x}Ni_xO_2$ solid solutions ($x>0.1$). In an interesting paper Barrio *et.al.*[22] suggested that the limit of solubility for Ce/Ni exchange is ~12%, whereas NiO phases were observed in samples with higher Ni loadings. On the other hand, Deraz[53] reported that diffraction peaks related to NiO can be observed for Ni concentrations of ~8%. Regarding the addition of copper it was reported that it increases the catalytic activity, selectivity and structural stability of Ni modified ceria.[19] Moreover, it is known that Cu can be incorporated into the ceria causing lattice contraction.[47] Nevertheless, our previous analyses suggests that, in the presence of nickel, copper atoms were not incorporated by the ceria lattice, forming segregated oxide phases instead. Thus, what are the possible reasons behind these interesting observations and what factors governs the segregation of oxide phases? It is clear that the composition can strongly influence the characteristics of those materials, but the analysis of the precise nature of the chemical structure and interactions at atomic level is difficult through experiments alone. Thus in the next session we address some of the issues raised, by using the DFT+U level of theory. Firstly, we carried out a systematic study on how the presence of Ni affects the ceria crystal structure by calculating the formation energies of the solid solutions and then we provide a reasonably accurate description of their local structure. Then, we assess how the addition of Cu lead to an overall oxide segregation rather to a further (Cu) incorporation into the lattice.

4.2. Computational Study

4.2.1 – General trends on the formation of $Ce_{1-x}Ni_xO_2$ solid solutions

In the fluorite-like CeO_2 crystal structure every Ce atom is arranged in a face-centered (*fcc*) unit cell surrounded by eight equivalent O atoms positioned in the vertices of a cube. The

equilibrium interatomic Ce-O bond length provided by our DFT+U calculations was found to be 2.377 Å, roughly larger than the experimental value (2.343 Å).[54] Furthermore, our DFT+U optimized lattice parameter (a_{DFT} = 5.490 Å) stand in good agreement with our experiments (a_{EXP} = 5.413 Å). Besides, the interlayer distances also present excellent agreement with our experimental data (see the inset Fig. 3). As mentioned a number of studies points out the beneficial effects of the interaction of ceria with Ni and Cu, however the chemical nature of these materials has not been fully established yet. So, firstly in order to shed light on the effect of the Ni incorporation into the CeO_2 crystal lattice we have tested various substitutional configurations constructed by exchanging Ce by Ni from 3.12% up to 18.75%, which means that the dopant dosages are realistic and somewhat in agreement with the maximum content of Ni identified experimentally by the XPS survey-scan (17%). We provided in Table 2 an overview of the calculated formation energies [ΔE_f (eV)] and the theoretically predicted lattice parameters [a_{DFT} (Å)]; where a_{DFT} values were obtained *via* $\sqrt[3]{V}/2$, being V the volume (Å^3) of the optimized supercells. As seen, aside from the heat of formation of CeO_2 (-10.01 eV) calculated from its elemental components and in excellent agreement with the literature,[25] all other values are positive suggesting that energy has to be driven to the systems in order to form solid solutions of the type $Ce_{1-x}Ni_xO_2$.

Table 2

A plot including the formation energies (ΔE_f) and the predicted lattice parameters versus the Ni load is shown in Fig. 5. Even though volume relaxation has been included in our calculations, it is interesting to note that in all cases the *fcc* crystal structure is conserved along the doping process. It starts with a lower endothermic energy of 2.75 eV as calculated for the $Ce_{0,9688}Ni_{0,0312}O_2$ system (3.12% of Ni), confirming that small amounts of Ni can be easily incorporated, and raises substantially along the incorporation of extra Ni atoms. In addition, the calculated lattice parameter

(a_{DFT}) is also a good indicator of the dependence of Ni incorporation with ΔE_f. Fig. 5 and Table 2 shows that a_{DFT} has only slightly decreased from "pure" CeO_2 (5.490 Å) to both $Ce_{0,9688}Ni_{0,0312}O_2$ (5.489 Å) and $Ce_{0,9375}Ni_{0,0625}O_2$ (5.480 Å), respectively. Here, we identified that both variations in a_{DFT} are highly consistent with our experimental data. Accordingly, they showed that the (experimental) formation of $NiCeO_\delta$ (see Table 1) resulted in a small contraction value of the lattice parameter (Δa_{EXP} = -0.006 Å); this value agrees well with the variations found for the lower-content Ni-doped system, $Ce_{0,9688}Ni_{0,0312}O_2$ (Δa_{DFT} = -0.001 Å) and particularly is in excellent agreement with $Ce_{0,9375}Ni_{0,0625}O_2$ (Δa_{DFT} = -0.010 Å). However, from this point a_{DFT} gradually decreased for systems with Ni content from 9.37% (Δa_{DFT} = -0.014 Å) until 18.75% (Δa_{DFT} = -0.033 Å). Moreover, it is interesting to note that ΔE_f increases almost linearly until Ni load of 9.37% (9.98 eV) and then it slightly rose until 12.5% (10.27 eV). On the other hand, by raising the Ni concentration above ~12% resulted in a sharp increase of ΔE_f as well as in strong lattice contractions, which in turn suggests that these compounds cannot be formed equivalently easily compared to $Ce_{0,9688}Ni_{0,0312}O_2$ and $Ce_{0,9375}Ni_{0,0625}O_2$. Therefore due to a combination of both effects (high ΔE_f and lattice shrinkage) the segregation of nickel oxide (NiO) would be expected to take place.

Figure 5

Overall, our theoretical and experimental results are consistent and suggest that the incorporation of Ni despite feasible[21] is governed by energetic and structural factors. In agreement, both experimental and theoretical (qualitatively) findings presuppose the existence of segregated NiO phase. The existence of NiO can be clearly identified experimentally from the diffraction peaks (Fig. 1). From the (theoretical) energetic and structural results we suggest that the formation of nanostructured Ce-Ni solid solution would be constrained to an amount around ~9.37 of Ni%, after which NiO phases tends to dominate principally because of the increasing energy necessary to replace Ce sites by Ni and of the considerable contraction of the ceria crystal lattice.

4.2.1.1 – On the Local Chemical Structure of $Ce_{1-x}Ni_xO_2$ Solid Solutions

Here we present a detailed discussion for a deeper insight into the local chemical structures. At first, we highlight low-content $NiCeO_\delta$ systems as illustrated by $Ce_{0,9688}Ni_{0,0312}O_2$ and $Ce_{0,9375}Ni_{0,0625}O_2$ supercells. For the first one, seen in Fig. 6 (A) and representing systems with Ni concentrations usually in the range of 3.12-6.25%, we observe that Ni assume a 4-fold coordination in the optimized $Ce_{0,9688}Ni_{0,0312}O_2$ supercell. The calculated formation energy (ΔE_f) of 2.75 eV was found to be in excellent agreement with the value provided by Wang *et.al.* (2.69 eV).[35] As discussed later, the local structure around the dopant is also important in determining the causes of lattice shrinking. Besides when larger amounts of Ni are added an interesting behavior is observed.

Figure 6

After testing various configurations we show in Fig. 6 (B) the energetically most stable structure derived from the 96-atom ($Ce_{0,9375}Ni_{0,0625}O_2$) supercell, which represents Ni doping that covers a range from 6.25% to 9.37%. This is in good agreement with the Ni chemical composition as determined by XPS (~10.6%). Furthermore, the system is very interesting for further theoretical studies because of the predicted variation of the lattice parameter (Δa_{DFT} = -0.010 Å) that is very similar to the experimental one (Δa_{EXP} = -0.006 Å), and due to its relatively low ΔE_f (5.98 eV). Interestingly, we observed that ΔE_f depends on the position of Ni in order to reach the energetically most stable structure. It can be seen in Fig. 6 that during the structural optimization the Ni coordination spheres have spontaneously moved from its initial location (nearest neighbor Ce sites) towards to the face of the O-cube. As a consequence, the Ni atoms adopted a nearly-planar 4-fold environment basically in a square pyramidal geometry, which is less symmetrical and less coordinated than the initial (8-fold) and is characterized by longer (1.850 Å) and shorter (1.812 Å) Ni-O bond lengths. Despite this fact, the most interesting feature is the appearance of an interaction of the type Ni-Ni pair with length of 2.525 Å, which is larger than the calculated Ce-O bond length

(2.377 Å) and shorter than the experimental value obtained for bulk NiO systems (2.960 Å).[55] As observed by our calculations the disturbance caused by the Ni-Ni pair may also induce a contraction of the lattice (Δa_{DFT} = -0.010 Å). As a matter of fact, the Ni-Ni bonding effect pushes away the opposite O-square which is now unbalanced by the Ni atoms displaced away from their initial position. Our DFT+U approach present a good agreement with previous experimental data. Barrio *et.al.* showed that a contribution around 1.8 Å in the EXAFS spectra relative to the radial distribution of local Ni neighbors in $Ce_{1-x}Ni_xO_2$ solid solutions is consistent with a strongly distorted Ni-O shell bond.[22] Furthermore, two characteristic Ni-O coordination distances as well as interactions of the type Ni-Ni were also suggested in their work.[22]

In general, our theoretical results can be extended to the systems containing higher Ni concentrations. In Fig. 7 (A-D) we show idealized solid solutions with 9.37% ($Ce_{0,9063}Ni_{0,0937}O_2$), 12.5% ($Ce_{0,875}Ni_{0,125}O_2$), 15.62% ($Ce_{0,8438}Ni_{0,1562}O_2$) and 18.75% ($Ce_{0,8125}Ni_{0,1875}O_2$) of Ni doping amount, respectively. It can be seen that the energetically most stable geometries were found when Ni replaces Ce nearest neighbor sites. However, our calculations have predicted that an excess of Ni inside the bulk favors the system destabilization due to a sharp increasing in ΔE_f and strong lattice contractions (see Fig. 5), inducing as a consequence the segregation of NiO. Furthermore, by increasing the amount of Ni [Fig. 7 (A-B)] the bond length of the Ni-Ni pair changed from 2.525 Å ($Ce_{0,9375}Ni_{0,0625}O_2$) to 3.166 Å ($Ce_{0,875}Ni_{0,125}O_2$), resembling more and more those found in NiO (3.05 Å).[55] In supercells with larger Ni amounts [Fig. 7 (C-D)], Ni domains are strongly disturbed due to lattice contraction, which causes Ni-Ni distances to vary widely (bond lengths so different as 2.289 Å to 4.593 Å were found). So, these systems (if considered as solid solutions) are highly instable and much probably they will not be formed; then the segregation of NiO phases is expected.

Figure 7

4.2.2 – On the Presence of Copper

As mentioned, various chemical processes can take advantage of the synergistic effect of Cu-Ce and Cu-Ni-Ce mixed oxides. However, at present little information is available concerning the chemical (local) structure and the energetic costs involved in the formation of these systems. Regarding our previous experimental findings it was suggested that Cu (added *a posteriori* to $NiCeO_{\delta}$) is preferably segregated in the form of oxide rather than incorporated by the lattice. Thus, it is important to investigate the reasons behind this interesting effect in order to understand at atomic level in which extent $NiCeO_{\delta}$ (see 4.1) is modified by Cu. Thus, aiming to find trends and to identify energetically stable structures a number of configurations were evaluated as indicated in Fig. 8. Based on our previous theoretical models (see item 4.2.1.1) and experimental findings we found quite reasonable to use the system $Ce_{0,9375}Ni_{0,0625}O_2$ [(Fig. 6 (B)] as a starting point to study the interaction with Cu atoms. In such a way, we seek for the best agreement with our experimental data by assuming that small amounts of Cu would be incorporated by the ceria crystal lattice, as observed by others.[47]

Figure 8

Table 3

Accordingly, we evaluate the following possibilities: (i) Cu is incorporated into $Ce_{0,9375}Ni_{0,0625}O_2$, which represents $NiCeO_{\delta}$, by replacing a Ce site and consequently an idealized solid solution of the type $Ce_{0,9063}Ni_{0,0625}\mathbf{Cu_{0,0312}}O_2$ is formed [Fig. 8 (A)]; or (ii) Cu is incorporated into $Ce_{0,9375}Ni_{0,0625}O_2$ forcing "half" of Ni to be expelled, then forming an structure of the type $Ce_{0,9375}Ni_{0,0312}\mathbf{Cu_{0,0312}}O_2$ [Fig. 8 (B)] and finally (iii) the incorporation of Cu expels all Ni from the bulk so that a solution of the type $Ce_{1-y}\mathbf{Cu_y}O_2$ (y = 0.0625) would be formed [Fig. 8 (C)]. According to the three possibilities analyzed, our calculations revealed that the higher formation energies shown in Table 3 makes all theoretical (idealized) solid solutions containing Cu energetically less

stable than those in which Cu is not present (see Table 2). In other words, the higher thermodynamic stability (lower formation energies) of the system saturated only by Ni ($Ce_{0,9375}Ni_{0,0625}O_2$) suggests that it has a tendency to "expel" Cu atoms. In turn, these results indicate that Cu atoms tend to segregate in the form of oxide (CuO) to the surface instead of move inside the lattice forming a ternary (Ce-Ni-Cu) solid solution. This is an interesting result and is in excellent (qualitative) agreement with our experimental data. As demonstrated previously in the subsection 4.1, CuO phases could be observed in the diffraction patterns and quantified by XPS analysis. It is important to note that despite our approximation do not explicitly account for interactions of the type Ni-Cu, it has been shown that the synergistic effect of these alloys on reduced surfaces is believed to be one of the causes of the increasing catalytic activity of Cu and Ni ceria-based systems.[19,56], which is in line with our theoretical findings which shows that Cu in energetically willing to form surface (active) species. Nevertheless, further studies are necessary in order to shed light on questions regarding the catalytic properties of these materials. In view of that, our preliminary (experimental) catalytic tests have shown that $NiCeO_\delta$ is highly active in preferential CO oxidation (PROX-CO) and that the catalytic activity is further enhanced by the addition of Cu (Cu-$NiCeO_\delta$); a detailed study is underway and will be published elsewhere.

5. CONCLUDING REMARKS

We have presented a combined experimental and theoretical (DFT+U) study in which some questions that concern the interaction between transition metals, namely Ni and Cu, with ceria (CeO_2) were addressed. Firstly, a comprehensive experimental characterization of the pure ceria as well as of the (Ni,Cu-modified) ceria-based materials, described as $NiCeO_\delta$ and Cu-$NiCeO_\delta$, has been performed. For the first one ($NiCeO_\delta$), where only Ni is present as a dopant, our experimental analyses (XRD, XRF, Raman, STEM and XPS) suggests that Ni species are able to interact with ceria by forming a solid solution through isomorphic substitution of Ce sites. Accordingly, it was observed that there is a limit (suggested to be around 9-10%) after which saturation is reached and

consequently the addition of extra Ni atoms causes no effect in the crystal structure of the solid solution, fostering the formation of surface domains identified as nickel oxide (NiO) phases. Then, our experimental findings have also shown that the addition of small amounts of Cu (6%) to $NiCeO_{\delta}$ (forming Cu-$NiCeO_{\delta}$) apparently can neither disturb the bulk structure nor force the incorporation of Cu atoms into the solid solution; the results suggest on the other hand that the Cu species also form segregated surface oxide (CuO) domains with a larger crystallite size (293 Å) when compared to NiO (285 Å).

Although our experimental investigation has provided valuable insight into the formation of a solid solution as well as identified the presence of surface (Ni,Cu) oxides, a complementary and more detailed picture of the (local) chemical structure was further achieved by DFT+U calculations. In general, our theoretical approach presented good agreement with the experimental findings being important in giving more accurate predictions into the factors shaping the solid solution formation and phase segregation. From a structural point of view, we have shown that the lattice parameter (theoretically) predicted for pure ceria is in excellent correspondence with its experimental counterpart. Furthermore, by analyzing modifications in the parameters predicted for Ni-doped theoretical models (compared to the "pure" ceria supercell model) with increasing Ni loading (from 3.12 up to 18.75 of Ni%), we could identify that a particular (idealized) structure (Δa_{DFT}= -0.010 Å) presents a close similarity with the experimental variation of the lattice parameter (Δa_{EXP}=-0.006 Å). From this structure, represented by the $Ce_{0,9375}Ni_{0,0625}O_2$ supercell, we could also recognize an important contribution from an interaction of the type Ni-Ni that in turn is strongly disturbed as the amount of Ni increases, usually above 9.37% (considering the idealized model); in qualitative terms it agrees well with the experimental findings. Moreover, our theoretical models have predicted strong contractions of the lattice parameters (substantially larger than the experimentally determined) in the supercells with Ni concentrations larger than 6.25-9.37 Ni%. From an energetic point of view, we show clear evidences that small amounts of Ni are easily incorporated by the ceria

lattice. On the other hand, by raising the concentration of Ni we observed a sharp increase of the formation energy principally for Ni amounts higher than 6.25-9.37 Ni%; high formation energies, together with lattice strong contractions, in turn have been associated as plausible causes for the segregation of both NiO and CuO (on Cu-$NiCeO_{\delta}$) phases to the surface of the grains and might be used as simple indicators of key factors for tailoring doped oxides containing controlled dopant concentrations.

AKNOWLEDGEMENTS

The authors would like to acknowledge the Brazilian agencies CNPq (EF Souza), CAPES (CAC) and Faperj for the financial support and Brazilian National Institute of Metrology (INMETRO).

6. REFERENCES

1 S. S. Lee, W. Song, M. Cho, H. L. Puppala, P. Nguyen, H. Zhu, L. Segatori and V. L. Colvin, *ACS Nano*, 2013, **7**, 9693–703.

2 M. Fernández-García, A. Martínez-Arias, J. C. Hanson and J. A. Rodriguez, *Chem. Rev.*, 2004, **104**, 4063–104.

3 T. X. T. Sayle, M. Cantoni, U. M. Bhatta, S. C. Parker, S. R. Hall, G. Möbus, M. Molinari, D. Reid, S. Seal and D. C. Sayle, *Chem. Mater.*, 2012, **24**, 1811–1821.

4 C.-M. Fan, L.-F. Zhang, S.-S. Wang, D.-H. Wang, L.-Q. Lu and A.-W. Xu, *Nanoscale*, 2012, **4**, 6835–40.

5 W. Huang and Y. Gao, *Catal. Sci. Technol.*, 2014, **4**, 3772–3784.

6 I. I. Soykal, H. Sohn and U. S. Ozkan, *ACS Catal.*, 2012, **2**, 2335–2348.

7 M. Tinoco, S. Fernandez-Garcia, M. Lopez-Haro, A. B. Hungria, X. Chen, G. Blanco, J. A. Perez-Omil, S. E. Collins, H. Okuno and J. J. Calvino, *ACS Catal.*, 2015, 3504–3513.

8 Z. Wu, V. Schwartz, M. Li, A. J. Rondinone and S. H. Overbury, *J. Phys. Chem. Lett.*, 2012, **3**, 1517–1522.

9 C. M. Y. Yeung, K. M. K. Yu, Q. J. Fu, D. Thompsett, M. I. Petch and S. C. Tsang, *J. Am. Chem. Soc.*, 2005, **127**, 18010–1.

10 K. Krishna, A. Bueno-López, M. Makkee and J. A. Moulijn, *Top. Catal.*, 2007, **42-43**, 221–228.

11 J. G. Nunan, M. J. Cohn and J. T. Dormer, *Catal. Today*, 1992, **14**, 277–291.

12 K. Zhou, X. Wang, X. Sun, Q. Peng and Y. Li, *J. Catal.*, 2005, **229**, 206–212.

13 W.-Q. Han, W. Wen, J. C. Hanson, X. Teng, N. Marinkovic and J. A. Rodriguez, *J. Phys. Chem. C*, 2009, **113**, 21949–21955.

14 J. Beckers and G. Rothenberg, *Dalton Trans.*, 2008, 6573–8.

15 E. Ramírez-Cabrera, A. Atkinson and D. Chadwick, *Appl. Catal. B Environ.*, 2002, **36**, 193–206.

16 O. H. Laguna, F. Romero Sarria, M. A. Centeno and J. A. Odriozola, *J. Catal.*, 2010, **276**, 360–370.

17 Q. Fu, H. Saltsburg and M. Flytzani-Stephanopoulos, *Science*, 2003, **301**, 935–8.

18 W. Y. Hernández, O. H. Laguna, M. A. Centeno and J. A. Odriozola, *J. Solid State Chem.*, 2011, **184**, 3014–3020.

19 E. T. Saw, U. Oemar, X. R. Tan, Y. Du, A. Borgna, K. Hidajat and S. Kawi, *J. Catal.*, 2014, **314**, 32–46.

20 J. A. Rodriguez, S. Ma, P. Liu, J. Hrbek, J. Evans and M. Pérez, *Science*, 2007, **318**, 1757–60.

21 G. Zhou, L. Barrio, S. Agnoli, S. D. Senanayake, J. Evans, A. Kubacka, M. Estrella, J. C. Hanson, A. Martínez-Arias, M. Fernández-García and J. A. Rodriguez, *Angew. Chemie*, 2010, **122**, 9874–9878.

22 L. Barrio, A. Kubacka, G. Zhou, M. Estrella, A. Martínez-Arias, J. C. Hanson, M. Fernández-García and J. A. Rodriguez, *J. Phys. Chem. C*, 2010, **114**, 12689–12697.

23 Z. Yang, L. Xie, D. Ma and G. Wang, *J. Phys. Chem. C*, 2011, **115**, 6730–6740.

24 J.-H. Lin, P. Biswas, V. V. Guliants and S. Misture, *Appl. Catal. A Gen.*, 2010, **387**, 87–94.

25 J. Paier, C. Penschke and J. Sauer, *Chem. Rev.*, 2013, **113**, 3949–85.

26 E. W. McFarland and H. Metiu, *Chem. Rev.*, 2013, **113**, 4391–427.

27 S. S.-Y. Lin, H. Daimon and S. Y. Ha, *Appl. Catal. A Gen.*, 2009, **366**, 252–261.

28 H. M. Rietveld, *J. Appl. Crystallogr.*, 1969, **2**, 65–71.

29 P. Giannozzi, *et.al.*, *J. Phys. Condens. Matter*, 2009, **21**, 395502.

30 J. P. Perdew, K. Burke and M. Ernzerhof, *Phys. Rev. Lett.*, 1996, **77**, 3865–3868.

31 D. Vanderbilt, *Phys. Rev. B*, 1990, **41**, 7892–7895.

32 S. R. Billeter, A. J. Turner and W. Thiel, *Phys. Chem. Chem. Phys.*, 2000, **2**, 2177–2186.

33 V. I. Anisimov, J. Zaanen and O. K. Andersen, *Phys. Rev. B*, 1991, **44**, 943–954.

34 M. Cococcioni and S. de Gironcoli, *Phys. Rev. B*, 2005, **71**, 035105.

35 X. Wang, M. Shen, J. Wang and S. Fabris, *J. Phys. Chem. C*, 2010, **114**, 10221–10228.

36 L. Szabová, M. F. Camellone, M. Huang, V. Matolín and S. Fabris, *J. Chem. Phys.*, 2010, **133**, 234705.

37 M. Huang and S. Fabris, *J. Phys. Chem. C*, 2008, **112**, 8643–8648.

38 M. Huang and S. Fabris, *Phys. Rev. B*, 2007, **75**, 081404.

39 P. R. L. Keating, D. O. Scanlon and G. W. Watson, *J. Mater. Chem. C*, 2013, **1**, 1093–1098.

40 K. M. Johansen, L. Vines, T. S. Bjørheim, R. Schifano and B. G. Svensson, *Phys. Rev. Appl.*, 2015, **3**, 024003.

41 D. E. P. Vanpoucke, P. Bultinck, S. Cottenier, V. Van Speybroeck and I. Van Driessche, *J. Mater. Chem. A*, 2014, **2**, 13723.

42 D. E. P. Vanpoucke, S. Cottenier, V. Van Speybroeck, I. Van Driessche and P. Bultinck, *J. Am. Ceram. Soc.*, 2014, **97**, 258–266.

43 Z. Yang, T. K. Woo and K. Hermansson, *J. Chem. Phys.*, 2006, **124**, 224704.

44 V. Sánchez Escribano, E. Fernández López, M. Panizza, C. Resini, J. M. Gallardo Amores and G. Busca, *Solid State Sci.*, 2003, **5**, 1369–1376.

45 V. Rives and S. Kannan, *J. Mater. Chem.*, 2000, **10**, 489–495.

46 S. Mahammadunnisa, P. Manoj Kumar Reddy, N. Lingaiah and C. Subrahmanyam, *Catal. Sci. Technol.*, 2013, **3**, 730–736.

47 P. Bera, K. R. Priolkar, P. R. Sarode, M. S. Hegde, S. Emura, R. Kumashiro and N. P. Lalla, *Chem. Mater.*, 2002, **14**, 3591–3601.

48 Y. Liu, X. Sun, Z. Zhou and Y. Lei, *J. Mater. Chem. A*, 2014, **2**, 14038.

49 W. Shan, *Appl. Catal. A Gen.*, 2003, **246**, 1–9.

50 X. Wang, J. A. Rodriguez, J. C. Hanson, D. Gamarra, A. Martínez-Arias and M. Fernandez-García, *J. Phys. Chem. B*, 2005, **109**, 19595–603.

51 W. Fang, C. Pirez, M. Capron, S. Paul, T. Raja, P. L. Dhepe, F. Dumeignil and L. Jalowiecki-Duhamel, *RSC Adv.*, 2012, **2**, 9626.

52 L. Pino, A. Vita, F. Cipitì, M. Laganà and V. Recupero, *Catal. Letters*, 2007, **122**, 121–130.

53 N. M. Deraz, *Ceram. Int.*, 2012, **38**, 747–753.

54 E. Kümmerle and G. Heger, *J. Solid State Chem.*, 1999, **147**, 485–500.

55. Wyckoff, R. W. G. Crystal Structures; Wiley & Sons: New York,1965; Vol. 1, pp 85-92.

56 J. A. Rodriguez and D. W. Goodman, *Science*, 1992, **257**, 897–903.

TABLES

Table 1 - Cell parameters, mean crystallite size of the materials obtained by Rietveld Refinement and chemical compositions obtained by XRF.

Material	Lattice Parameter (Å)	Crystallite Size (Å)			Chemical Composition (wt.%)	
		CeO_2	NiO	CuO	Ni	Cu
CeO_2	5.413	93	-	-	-	-
$NiCeO_\delta$	5.407	104	253	-	18	-
$Cu\text{-}NiCeO_\delta$	5.407	102	285	293	22	6.2

Table 2 – Calculated DFT+U formation energies and theoretically predicted lattice parameters for the idealized Ni-doped ceria supercells.

Ni(%)	System	ΔE_f (eV)	V(Å^3)	a_{DFT} (Å)
0	CeO_2	-10.01	1324.067	5.490
3.12	$Ce_{0,9688}Ni_{0,0312}O_2$	2.75	1323.331	5.489
6.25	$Ce_{0,9375}Ni_{0,0625}O_2$	5.98	1316.209	5.480
9.37	$Ce_{0,9063}Ni_{0,0937}O_2$	9.92	1313.020	5.476
12.50	$Ce_{0,875}Ni_{0,125}O_2$	10.27	1307.452	5.467
15.62	$Ce_{0,8438}Ni_{0,1562}O_2$	13.57	1306.049	5.465
18.75	$Ce_{0,8125}Ni_{0,1875}O_2$	15.10	1300.148	5.457

Table 3 - Calculated DFT+U formation energies and lattice parameters for the idealized (Ni,Cu) supercells.

(%) Ni+Cu	System	ΔE_f(eV)	a_{DFT}(Å)
Ni(3.12%) + Cu(3.12%)	$Ce_{0,9375}Ni_{0,0312}Cu_{0,0312}O_2$	10.46	5.481
Ni(6.25%) + Cu(3.12%)	$Ce_{0,9063}Ni_{0,0625}Cu_{0,0312}O_2$	11.44	5.480
Cu (6.25 %)	$Ce_{0,9375}Cu_{0,0625}O_2$	11.92	5.459

FIGURE CATPTIONS

Figure 1 – Powder X-ray diffraction (XRD) patterns of pure CeO_2, $NiCeO_\delta$ and Cu-$NiCeO_\delta$ materials.

Figure 2 – Raman spectra of the ceria-based materials.

Figure 3 – Representative STEM micrograph relative to the Cu-modified $NiCeO_\delta$. The smaller inset graph represents a selected area attributed to the NiO phase, while the larger inset represents an idealized ceria crystal structure obtained through DFT+U calculations (where the numbers indicate the plane distances in Å).

Figure 4 – Typical XPS survey-scan for the as-prepared Cu-$NiCeO_\delta$ (A) and $NiCeO_\delta$ (B) systems. The insets I and II in 'A' represents a magnification of the XPS spectra relative to Cu 2p and Ni 2p core level regions. The inset in 'B' represents a magnified XPS spectrum relative to the Ni 2p core level.

Figure 5 – The left side (black balls) shows the correlation between the formation energy (ΔE_f) and the amount of Ni inside the ceria bulk. The right side (red squares) represent the theoretically predicted lattice parameters of the solid solutions. Here both dashed (black) and solid (red) lines are fits of the data points depicted in order to be a guide to the eyes.

Figure 6 – Ball and stick model-structures corresponding to the $Ce_{0,9688}Ni_{0,0312}O_2$ (A) and $Ce_{0,9375}Ni_{0,0625}O_2$ (B) supercells (idealized solid solutions) with 3.12 and 6.25 of Ni% isomorphic substitution. Dashed circles (green) represent nearest neighbor sites and indicate the initial position of the Ni dopants, which replaced Ce sites and were allowed to freely relax. White and red spheres represent Ce and O atoms, respectively.

Figure 7 – Ball and stick models representing idealized supercells with 9.37 (A), 12.5 (B), 15.6 (C) and 18.75% (D) of Ni. Green spheres (representing Ni atoms) were placed (through isomorphic substitutions) in nearest neighbor Ce positions. White and red spheres represent Ce and O atoms, respectively.

Figure 8 – Ball and stick models representing idealized $Ce_{1-x-y}Ni_xCu_yO_2$ supercells containing equal amount (3.12%) of both Ni and Cu (A), 6.25% and 3.12% of Ni and Cu, respectively (B), and 6.25 of Cu% (C). Orange and green spheres are associated to Cu and Ni atoms, respectively, while white and red spheres represent Ce and O atoms, respectively.

FIGURES

Figure 1

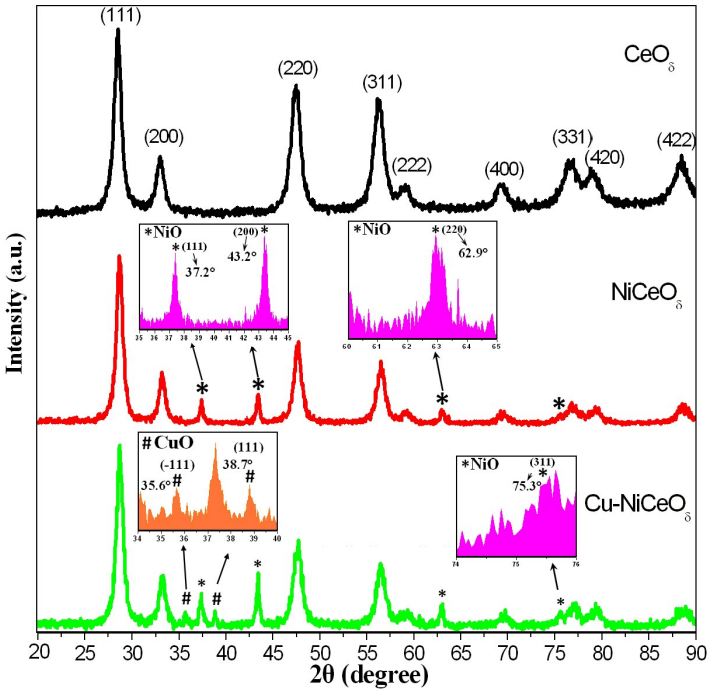

Figure 2

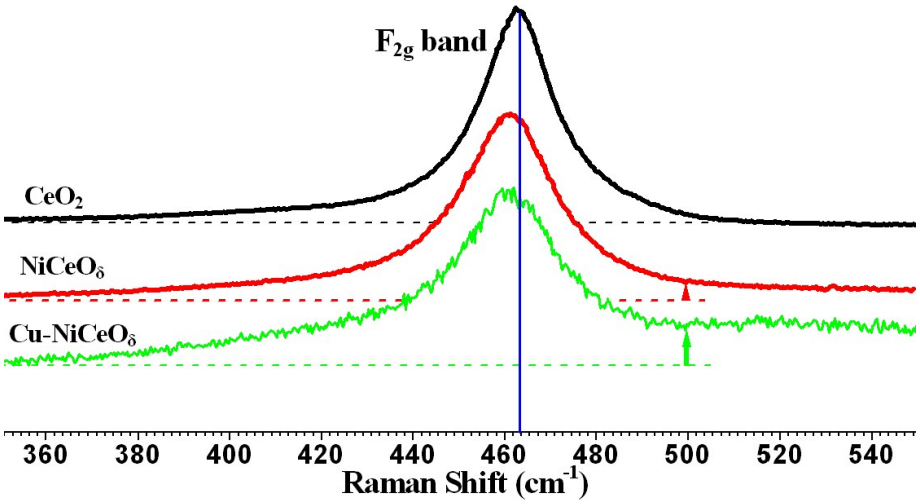

Figure 3

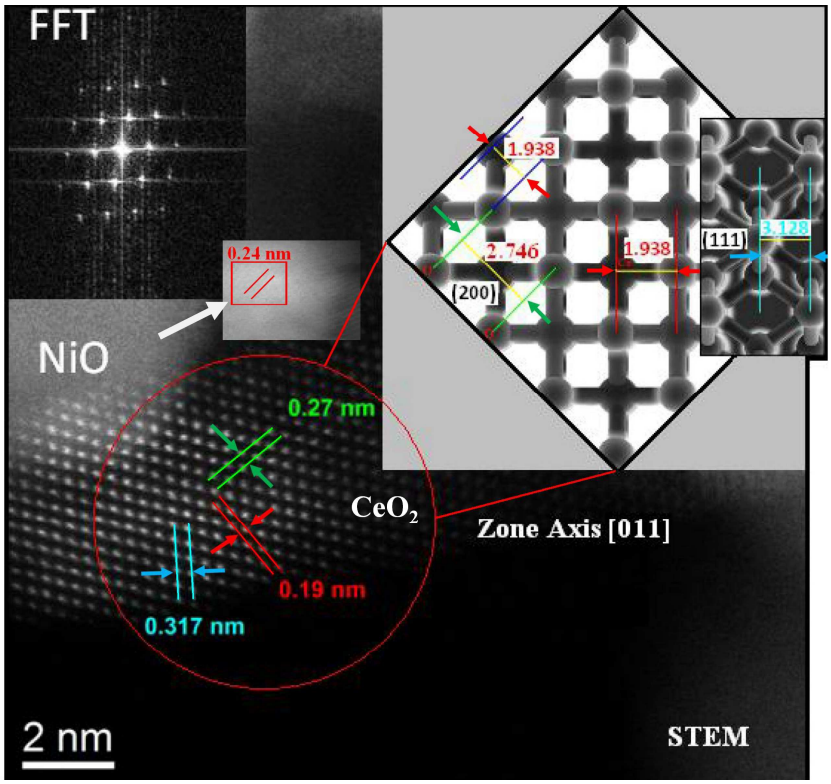

Figure 4

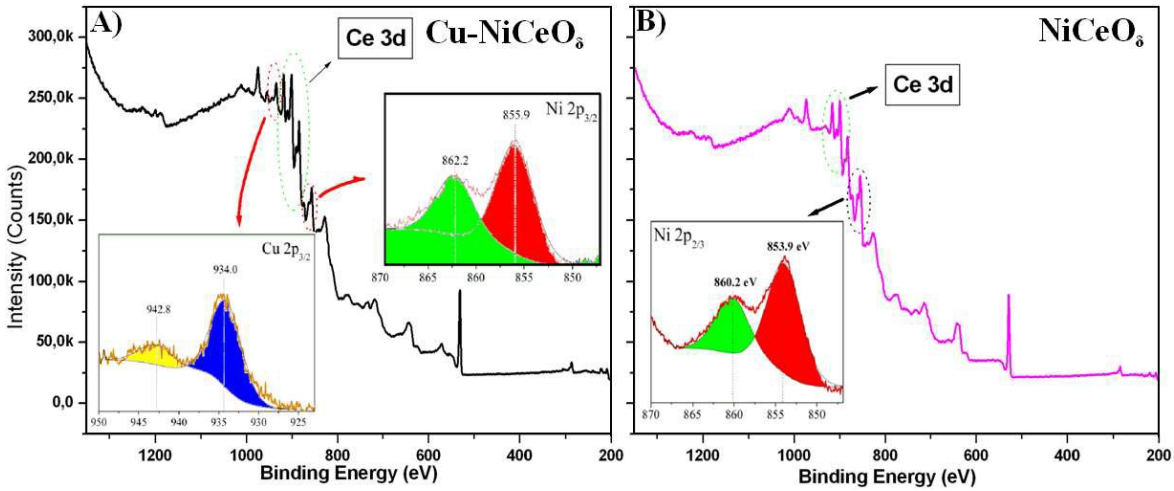

Figure 5

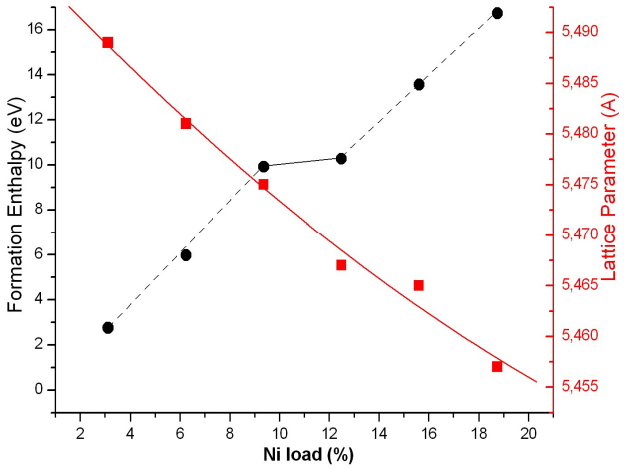

Figure 6

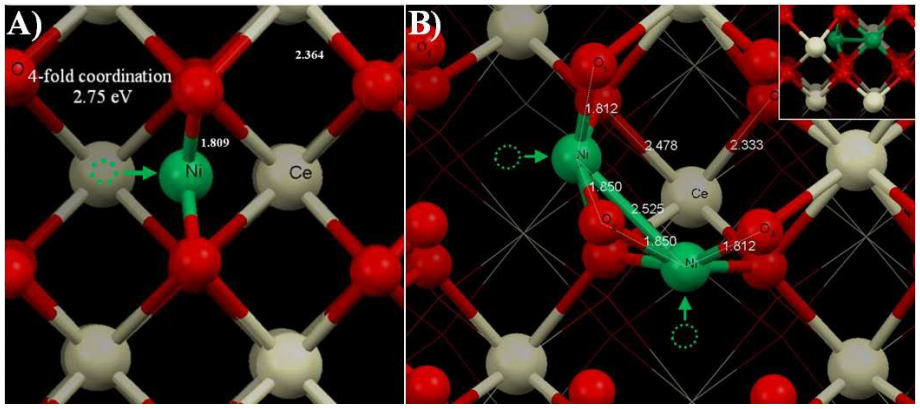

Figure 7

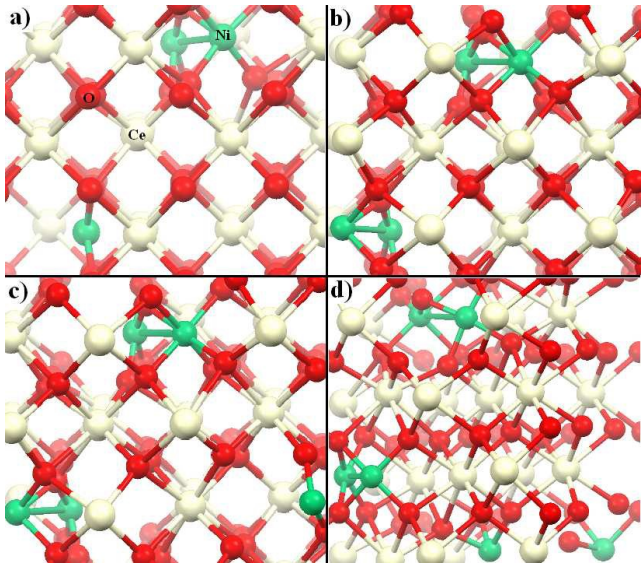

Figure 8

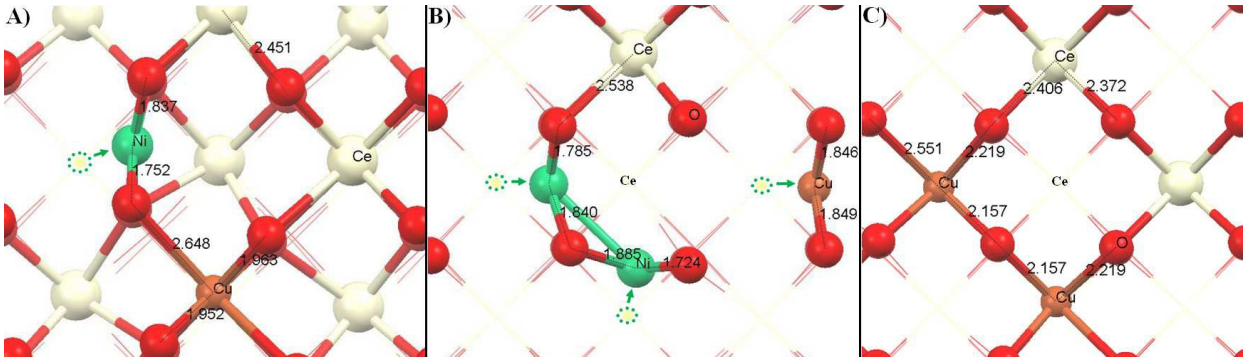

GRAPHICAL ABSTRACT